NANO LETTERS

pubs.acs.org/NanoLett

Thermal Transport in Suspended and Supported Monolayer Graphene Grown by Chemical Vapor Deposition

Weiwei Cai,† Arden L. Moore,† Yanwu Zhu, Xuesong Li, Shanshan Chen, Li Shi,* and Rodney S. Ruoff*

Department of Mechanical Engineering and Texas Materials Institute, University of Texas at Austin, Austin, Texas 78712

ABSTRACT Graphene monolayer has been grown by chemical vapor deposition on copper and then suspended over a hole. By measuring the laser heating and monitoring the Raman G peak, we obtain room-temperature thermal conductivity and interface conductance of (370 + 650/−320) W/m K and (28 + 16/−9.2) MW/m^2 K for the supported graphene. The thermal conductivity of the suspended graphene exceeds (2500 + 1100/−1050) W/m K near 350 K and becomes (1400 + 500/−480) W/m K at about 500 K.

KEYWORDS Thermal conductivity, thermal interface resistance, graphene, Raman, measurement

Since graphene was exfoliated from graphite in 2004,[1] the two-dimensional monatomic sheet has attracted increased interest for both fundamental studies and applications in high-speed electronic devices, sensors, memory, and spintronic devices among others.[2] Because it is difficult to utilize mechanically exfoliated, small graphene flakes for mass production of functional devices, there have been intense efforts to develop methods for synthesis of large-area, high-quality graphene, including thermal decomposition from SiC or chemical vapor deposition (CVD) on a thin film transition metal catalyst such as Ni or Cu.[3−6] Electron transport measurements have found that the charge mobility of as-synthesized graphene depends on the grain size. For graphene grown by CVD on Cu, the mobility can reach about 4050 cm^2 V^{-1} s^{-1},[6] which is about 4 times smaller than the highest value of about 15000 cm^2 V^{-1} s^{-1} found in mechanically exfoliated graphene supported on SiO_2 at room temperature.[1,7−9] On the other hand, the thermal conductivity remains unknown for these large-area CVD graphene, which can be scaled up for thermal management applications more readily than exfoliated graphene flake.

Although electron transport in graphene has been studied extensively and graphene is predicted to have very high thermal conductivity near room temperature,[10−13] there have been only limited experimental data in the literature on phonon transport in graphene because of experimental challenges. In a recent experiment based on micro-Raman spectroscopy, a thermal conductivity value of about 5000 W/m K was found for a ∼20 μm long monolayer graphene flake with a ∼3 μm long suspended segment obtained by micromechanical exfoliation of graphite.[14] This value is about two times higher than values found in diamond and graphite in the basal plane.[15] This measurement method is based on the dependence of the Raman G peak frequency on the temperature of the flake heated by the Raman laser.[14,16] An optical absorption of ∼6% per pass of the laser beam was determined based on an optical absorption model in conjunction with a calibration with graphite. This number is considerably higher than the 2.3% value obtained from an optical transmission measurement of monolayer graphene.[17] While the discrepancy could be attributed to sample contamination and different absorption coefficients at different wavelengths,[11] it is desirable to measure the optical absorption directly. In addition, heat loss from the graphene to the SiO_2 substrate at the two ends of the trench was neglected for this measurement and the thicker graphite region was assumed to be a perfect heat sink. Consequently, the thermal conductivity of the monolayer segment supported on SiO_2 was assumed to be the same as that of the suspended segment. However, a recent experiment shows that the thermal conductivity of graphene supported on SiO_2 could be considerably lower than values for the suspended graphene due to phonon leakage across the graphene−substrate interface.[18] Hence, it is necessary to re-evaluate the thermal contact of the supported graphene segment to better understand the intrinsic thermal conductivity of suspended graphene.

In this letter, we report a different approach based on micro-Raman spectroscopy for the measurement of the thermal conductivity of large-area, monolayer graphene grown by CVD on copper[6] and subsequently suspended over a circular hole. The obtained room-temperature thermal conductivity and thermal interface conductance for the supported area of the CVD graphene are comparable to the

* To whom correspondence should be addressed. E-mail: (RSR) r.ruoff@mail.utexas.edu; (LS) lishi@mail.utexas.edu.

† These authors contributed equally to this work.

Received for review: 12/18/2009
Published on Web: 04/20/2010

DOI: 10.1021/nl9041966 | *Nano Lett.* **2010,** *10,* 1645–1651

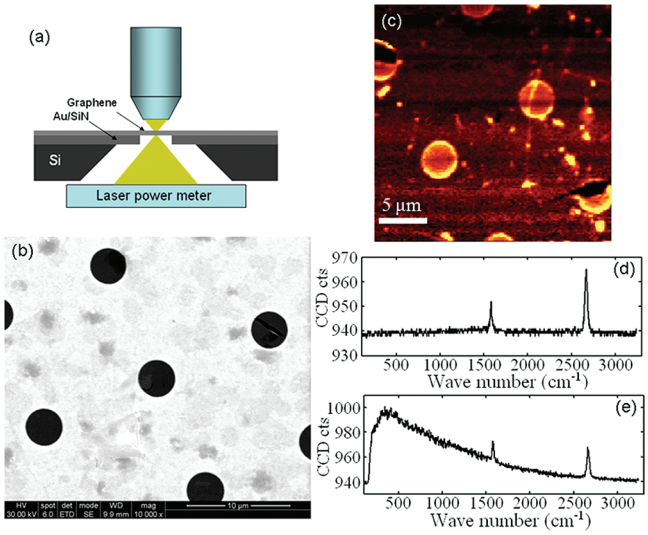

FIGURE 1. (a) Schematic of the experimental setup for graphene thermal conductivity measurement. (b) The scanning electron microscopy image and (c) micro-Raman G peak map of the suspended graphene on the Au-coated SiN_x porous membrane. Raman spectra of suspended graphene (d) and graphene on the Au-coated SiN_x support (e) show the G peak and 2D peak features characteristic of monolayer graphene.

recently reported values for mechanically exfoliated graphene on SiO_2. The thermal conductivity of the suspended region of the CVD graphene is higher than the reported values for graphite at near room temperature and 500 K, respectively.

The sample used in the thermal measurement was large-area high-quality monolayer graphene grown on 25 μm thick Cu foils using a CVD method that we demonstrated recently.[6] The surface of the graphene-on-Cu was coated with poly(methyl methacrylate) (PMMA) followed by curing. After the Cu substrate was dissolved in an $Fe(NO_3)_3$ solution (1 M/L), the PMMA-graphene was lifted up from the solution and transferred to the Au-coated surface of a 300 nm thick, 0.5 × 0.5 mm^2, low-stress silicon nitride (SiN_x) membrane supported on a circular 3 × 3 mm^2 silicon frame.[19] The SiN_x membrane consists of a 100 × 100 array of 3.8 μm diameter holes at a pitch of 10 μm between holes. The thermal conductivity of SiN_x is about ~5 W/m K and rather low. To increase the thermal conductance of the membrane that serves as a heat sink for this measurement, a ~500 nm thick Au film was evaporated on the SiN_x surface prior to the graphene transfer. After the transfer, the PMMA was removed in acetone. Figure 1a shows a schematic diagram of the obtained graphene suspended over a through hole in the Au-coated SiN_x support. The SEM image in Figure 1b shows a graphene flake that covers holes in the Au/SiN_x membrane. Some cracks can be observed in some areas of the flake.

The quality and the number of (stacked) layers of the graphene films were determined by micro-Raman spectroscopy.[6] Figure 1c shows a 25 × 25 μm^2 Raman mapping image of the G peak intensity of the graphene on SiN_x support. The Raman image clearly shows the existence of suspended graphene on the holes. On some holes, the film is broken or wrinkled. We have chosen graphene areas without such visible defects for the thermal measurement. As shown in Figure 1d,e, the typical Raman spectra obtained from the chosen suspended graphene do not contain the D Band associated with defects[6] and indicate high-quality monolayer graphene. In comparison, the relatively high background level in the Raman spectrum of the supported graphene comes from the Au coating on the SiN_x support.

During the thermal measurement, a 532 nm laser beam is focused using an objective lens on either the center of the suspended graphene or the area of the graphene supported on the Au/SiN_x membrane. In this configuration, the heat flux vector is along the radial direction away from the center of the graphene so as to match the radial symmetry of the laser beam. The optical transmission through the suspended graphene is measured using a semiconductor laser power meter (Newport, Model 1918-c) placed under the SiN_x support, as illustrated in Figure 1a. The laser beam size is much smaller than the diameter of the holes, as discussed below. Because it has been reported that the reflection by the graphene flake is less than 0.1% and is negligible,[17] the power (Q) absorbed by the suspended graphene is obtained as the difference between the power transmitted through an empty hole (P_{empty}) and that transmitted through a graphene flake ($P_{graphene}$), that is, $Q = P_{empty} - P_{graphene}$. The obtained optical absorption of 3.3 ± 1.1% at 532 nm wavelength is comparable to the 2.3% value reported for 550 nm wavelength in the literature.[17] At the same incident laser power, the absorbed laser power by the supported graphene is taken as twice of that measured on the suspended graphene because of the reflection from the Au surface.

The temperature rise in the optically heated graphene causes red-shift of the G peak because of bond softening. It has been shown that the red shift of the Raman G peak of graphene linearly depends on the sample temperature.[20] To calibrate the relationship between the Raman shift and the temperature rise, we obtained Raman spectra of the graphene sample when the sample was placed on a heating stage with its temperature measured by a thermocouple. On the basis of 12 measurements on both supported and suspended graphene areas, two of which are shown in the inset of Figure 2, the Raman G peak down shifts with increasing stage temperature at a rate of (4.05 ± 0.2) × 10^{-2} cm^{-1}/K. We estimate that stress caused by thermal expansion mismatch resulted in Raman shift one order of magnitude smaller than this measurement value. Hence, this value is used to determine the graphene temperature from the G peak position when the graphene is heated by the Raman laser at different powers and the stage is kept at ambient temperature. Figure 2 shows the relationship between the measured graphene temperature rise and the absorbed power when the laser beam is focused on either the supported graphene or the center of the suspended graphene with the use of the 100× and 50× objectives. The measured Raman shift is much smaller when the laser beam is focused

DOI: 10.1021/nl9041966 | *Nano Lett.* **2010,** *10,* 1645–1651

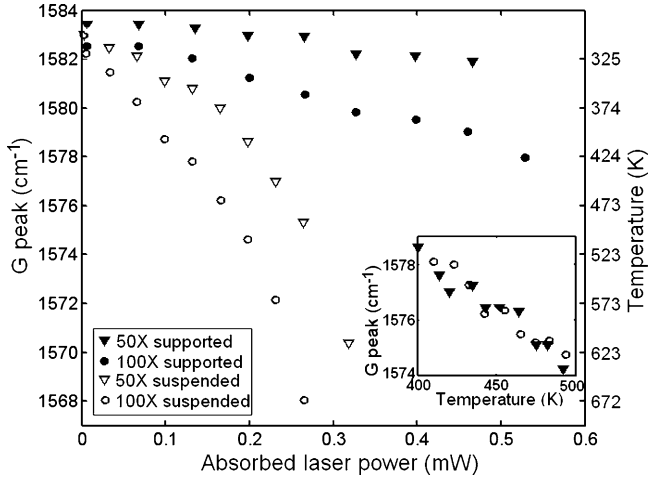

FIGURE 2. The G peak shift (left axis) and temperature (right axis) measured on the supported graphene and at the center of the suspended graphene with the 100× and 50× objectives as a function of the absorbed laser power when the stage temperature is kept at room temperature. The inset shows that the red shift of the Raman G peak measured with low laser power on both supported and suspended graphene as a function of the stage temperature.

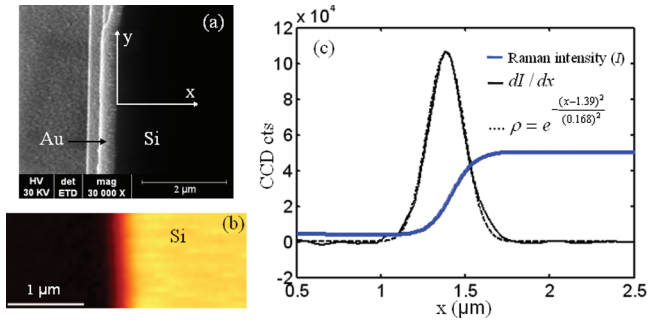

FIGURE 3. (a) The scanning electron microscopy image and (b) 3 μm × 1 μm micro-Raman map across a Au-coated sharp Si edge. (c) The Raman intensity (blue) and extracted profile of the laser beam (black) as a function of the beam position.

on the supported graphene than at the center of the suspended graphene because heat transfer from the supported graphene to the Au support results in lower temperature rise in the supported graphene than in the suspended graphene.

The thermal measurement requires a careful determination of the radius of the laser beam spot (r_0), which is obtained by performing a micro-Raman scan across a smooth cleaved edge of a Si substrate. Figure 3a,b shows a scanning electron microscopy image of the Si edge and a 1 μm × 3 μm micro-Raman image integrated from the 490 to 550 cm^{-1} frequency range of the Si peak obtained with the 100× objective. Au film of about 200 nm in thickness was evaporated on the side of the freshly cleaved Si edge to eliminate the Raman signal from the cleaved edge. The Si peak is much higher than the Au background, which is not included in the integrated intensity of the Si peak. Here, the measured intensity (I) of the silicon peak at ~520 cm^{-1} is proportional to the total laser power incident on the silicon wafer. Figure 3c shows the measured I as a function of the distance (x) of the laser beam from the cleaved edge. Instead of the more complicated Airy pattern, a Gaussian function $\exp(-x^2/r_0^2)$ can be used to fit the slope dI/dx to obtain the beam size r_0. This procedure yields $r_0 = 0.17$ and 0.28 μm for the 100× and 50× objectives. These r_0 values are close to the calculated values of 0.19 and 0.24 μm using $r_0 = \lambda/\pi$NA, where NA is the numerical aperture value of 0.9 and 0.75 for the 100× and 50× objectives, respectively.

We calculate that direct laser heating of the Au film produces a negligible rise in the film temperature.[21] Hence, the temperature rise measured with the laser beam on the supported graphene is caused by optical absorption by the supported graphene. For the supported graphene, substrate interaction can reduce the mean free paths of phonons in graphene, especially the long-wavelength phonons, to be smaller than the laser beam size.[18] In this case, diffusive phonon transport in the supported graphene makes it possible to obtain the temperature (T) distribution from the following heat diffusion equation in the cylindrical coordinate

$$\frac{1}{r}\frac{d}{dr}\left(r\frac{dT}{dr}\right) - \frac{g}{\kappa_s t}(T - T_a) + \frac{\dot{q}'''}{\kappa_s} = 0 \qquad (1)$$

where T_a is the ambient temperature, r is the radial position measured from the center of the laser beam, $t = 0.335$ nm is the graphene thickness, κ_s is the thermal conductivity of the supported graphene, which can be different from the thermal conductivity (κ) of the suspended graphene, and g is the total interface thermal conductance per unit area between the graphene and the Au-covered support as well as the surrounding air molecules. In eq 1, $\dot{q}'''$ is the volumetric optical heating and given as

$$\dot{q}''' = \frac{q_0''}{t}\exp\left(-\frac{r^2}{r_0^2}\right) \qquad (2)$$

where q_0'' is the peak absorbed laser power per unit area at the center of the beam spot. The total absorbed laser power Q is then

$$Q = \int_0^\infty q_0'' \exp\left(-\frac{r^2}{r_0^2}\right)2\pi r\, dr = q_0''\pi r_0^2 \qquad (3)$$

With the use of $\theta \equiv (T - T_a)$ and $z = (g/\kappa_s t)^{1/2} r$, eq 1 becomes a nonhomogeneous Bessel's equation

$$\frac{\partial^2\theta}{\partial z^2} + \frac{1}{z}\frac{\partial\theta}{\partial z} - \theta = -\frac{q_0''}{g}\exp\left(-\frac{z^2}{z_0^2}\right) \qquad (4)$$

DOI: 10.1021/nl9041966 | Nano Lett. 2010, 10, 1645–1651

The solution to eq 4 is given as[22]

$$\theta(z) = C_1 I_0(z) + C_2 K_0(z) + \theta_p(z) \quad (5)$$

where the two homogeneous solutions $I_0(z)$ and $K_0(z)$ are the zero-order modified Bessel functions of the first and second kind, respectively. The particular solution is obtained using the variation of parameters method as[22]

$$\theta_p(z) = I_0(z) \int \frac{K_0(z)\frac{q_0''}{g}\exp\left(-\frac{z^2}{z_0^2}\right)}{-I_0(z)K_1(z) - K_0(z)I_1(z)} \times dz - K_0(z) \int \frac{I_0(z)\frac{q_0''}{g}\exp\left(-\frac{z^2}{z_0^2}\right)}{-I_0(z)K_1(z) - K_0(z)I_1(z)} dz \quad (6)$$

where $I_1(z)$ and $K_1(z)$ are the first-order modified Bessel functions of the first and second kind, respectively. The boundary conditions $(d\theta)/(dz)|_{z=0} = 0$ and $\theta(z\rightarrow\infty) = 0$ yield $C_2 = 0$ and $C_1 = -\lim_{z\rightarrow\infty}(\theta_p(z))/(I_0(z))$, which approaches a constant value for large z.

The temperature rise in the graphene measured by the Raman laser beam is

$$\theta_m = \frac{\int_0^\infty \theta(r)\exp\left(-\frac{r^2}{r_0^2}\right) r\, dr}{\int_0^\infty \exp\left(-\frac{r^2}{r_0^2}\right) r\, dr} \quad (7)$$

We define the measured thermal resistance as $R_m \equiv \theta_m/Q$. On the basis of eqs 3 and 7

$$R_m = \frac{\int_0^\infty \left(-I_0(z)\lim_{z\rightarrow\infty}\frac{\theta_p(z)}{I_0(z)} + \theta_p(z)\right)\exp\left(-\frac{r^2}{r_0^2}\right) r\, dr}{\int_0^\infty \exp\left(-\frac{r^2}{r_0^2}\right) r\, dr \int_0^\infty q_0'' \exp\left(-\frac{r^2}{r_0^2}\right) 2\pi r\, dr} \quad (8)$$

Figure 2 shows approximately linear θ_m and Q relations for the supported graphene, the slopes of which yield R_m values of $(2.37 \pm 0.81) \times 10^5$, and $(1.05 \pm 0.37) \times 10^5$ K/W, respectively, for the 100× and 50× objective lens. The uncertainties in the R_m values include both the calibration or bias errors of θ_m and Q and the random uncertainty in five measurements of the θ_m versus Q slopes. Only the random uncertainties need to be propagated into that of the ratio between the two R_m values with the two objectives.[23] This ratio is determined to be 2.26 ± 0.23. On the basis of eq 8, this ratio only depends on the g/κ_s ratio and can be used to determine g/κ_s uniquely. The κ_s and g values are further determined from the R_m value measured with one of the objective lens. The procedure yields κ_s of $(370 + 650/-320)$ W/m K and g of $(28 + 16/-9.2)$ MW/m^2 K. The κ_s value is comparable to the room-temperature thermal conductivity range of 479−680 W/m K recently measured for exfoliated graphene supported on SiO_2.[18] The g value is also comparable to the reported thermal interface conductance values of ∼50 and 83 MW/m^2 K between graphite and evaporated Al and for graphene embedded in SiO_2,[24,25] respectively, and much larger than the interface thermal conductance between the graphene and surrounding air molecules.[26]

When the laser beam is focused on the center of the suspended graphene, the measured thermal resistance becomes

$$R_m = R_g + R_c \quad (9)$$

where $R_g \equiv (T_m - T_1)/Q$ is defined as the equivalent thermal resistance of the suspended graphene here although thermal resistance is usually not used for regions of heat generation, $R_c \equiv (T_1 - T_a)/Q$ is the contact thermal resistance between the supported graphene and the membrane, and T_1 is the temperature at the edge of the suspended graphene. Because the 1.9 μm hole radius (R) is much larger than the beam size r_0 values of 0.17 and 0.28 μm, the optical heating term $\dot{q}'''$ in eq 1 can be neglected for the supported graphene region of $r > R$. With $\dot{q}''' = 0$, the temperature distribution for $r > R$ is given by the homogeneous solution components of eq 5.[27] With the use of the boundary conditions $\theta(z\rightarrow\infty) = 0$ and $Q(1 - \exp(-R^2/r_0^2)) = -2\pi R t \kappa_s (\partial T/\partial r)|_R$, we obtain the temperature distribution in the supported area of the graphene as

$$\theta(z) = \frac{Q(1 - \exp(-R^2/r_0^2))}{2\pi R\sqrt{gt\kappa_s}}\frac{K_0(z)}{K_1(z_R)}, \quad \text{for } r \geq R \quad (10)$$

where z_R is the value of z at $r = R$. The thermal contact resistance is obtained as

$$R_c = \frac{\theta(z_R)}{Q(1 - \exp(-R^2/r_0^2))} = \frac{1}{2\pi R\sqrt{gt\kappa_s}}\frac{K_0(z_R)}{K_1(z_R)} \quad (11)$$

With the above-obtained κ_s and g values, $R_c \approx (4.4 + 8.4/-2.0) \times 10^4$ K/W.

DOI: 10.1021/nl9041966 | Nano Lett. 2010, 10, 1645–1651

If phonon transport is diffusive in the suspended region of the graphene monolayer and heat loss from the graphene to surrounding air and via radiation is ignored,[26] the temperature distribution in the suspended graphene can be obtained by integrating eq 1 for the case of $g = 0$. With the boundary conditions of $T(r = R) = T_1$ and $Q(1 - \exp(-R^2/r_0^2)) = -2\pi R\kappa t(\mathrm{d}T/\mathrm{d}r)|_R$, the resulting temperature distribution in the suspended graphene is obtained as

$$T(r) = T_1 + \frac{Q}{2\pi\kappa t}\ln\left(\frac{R}{r}\right)\beta(r), \quad \text{for } r \le R \tag{12}$$

where

$$\beta(r) = \left[1 + \frac{Ei(-r^2/r_0^2) - Ei(-R^2/r_0^2)}{2\ln\left(\frac{R}{r}\right)}\right] \tag{13}$$

where $Ei(x)$ is the exponential integral.

The graphene temperature measured by the Raman laser is approximated as

$$T_m \approx \frac{\int_0^R T(r)\exp\left(-\frac{r^2}{r_0^2}\right)r\,\mathrm{d}r}{\int_0^R \exp\left(-\frac{r^2}{r_0^2}\right)r\,\mathrm{d}r} \tag{14}$$

For this diffusive transport analysis, the equivalent thermal resistance of the suspended graphene is obtained as

$$R_g \equiv \frac{T_m - T_1}{Q} = \alpha\frac{\ln(R/r_0)}{2\pi\kappa t} \tag{15}$$

where

$$\alpha = \frac{T_m - T_1}{T_0 - T_1}\beta(r_0) \tag{16}$$

Here T_0 is the temperature at $r = r_0$ and the ratio $(T_m - T_1)/(T_0 - T_1)$ is a function of r_0 only and found using eqs 12−14 to increase from 1.02 to 1.03 when r_0 increases from 0.17 to 0.28 μm. With $R = 1.9$ μm, the α factor is 0.98 and 0.97 based on the measured r_0 value of 0.17 and 0.28 μm for the 100× and 50× objective lens, respectively.

Because of the nonlinear T_m versus Q behavior shown in Figure 2 for the suspended graphene at high T_m values, we calculate $R_m = (T_m - T_a)/Q$ for each data point instead of the slope of the T_m versus Q curve. The obtained R_m values are plotted versus $\alpha\ln(R/r_0)$ in Figure 4 for three sets of data with $T_m \approx 370$, 430, and 465 K, respectively. The R_m values are 1 order of magnitude larger than the above-obtained R_c value. The relatively small R_c is attributed to the large contact area achieved in the radial heat flow geometry compared to an axial heat flow pattern. On the basis of eqs 9 and 15, R_m is expected to decrease with $\alpha\ln(R/r_0)$ linearly and equals the R_c value at $\alpha\ln(R/r_0) = 0$. However, linear extrapolation of the two measured data with a similar T_m in Figure 4 to $\alpha\ln(R/r_0) = 0$ yields a negative resistance, the magnitude of which decreases with increasing T_m. We attribute this behavior to quasi-ballistic transport of low-frequency phonons that have mean free paths (l) longer than the r_0 value of 0.17 or 0.28 μm.[28] Photoexcited electron−hole pairs loss energy to high-frequency phonons on a time scale of 100 fs,[29] corresponding to a length scale of 100 nm that is comparable to or smaller than the two r_0 values. On the other hand, low-frequency phonons with $l > r_0$ are not thermalized within r_0 and thus carry less heat than that assumed in the diffusive transport analysis. Consequently, R_g consists of an additional ballistic resistance component (R_b) in addition to the diffusive component (R_d) given in eq 15, that is, $R_g \approx R_d + R_b$.[30−34] Because R_b is proportional to the Knudsen number $K \equiv l/r_0$, the measured R_g consists of a larger relative contribution from R_b for the smaller r_0, giving rise to the negative intercept at $\alpha\ln(R/r_0) = 0$ of Figure 4. The magnitude of this negative intercept decreases with increasing T_m because increased anharmonic phonon scattering reduces l of low-frequency phonons.

With the ballistic resistance component ignored, we calculate the lower bound of the thermal conductivity of the suspended graphene as

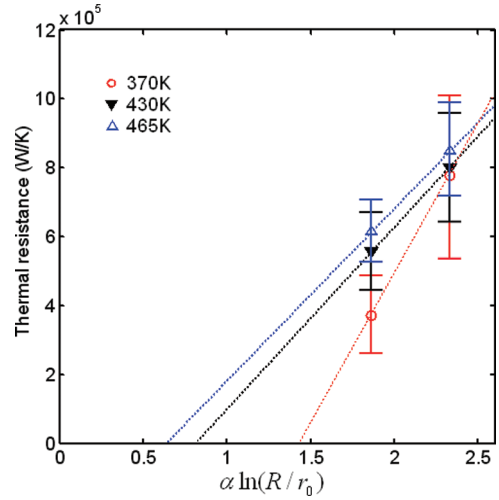

FIGURE 4. The measured thermal resistance values as a function of $\alpha\ln(R/r_0)$. The lines are a linear fit to each pair of the measurement data obtained at the same measured graphene temperature of 370, 430, and 465 K, respectively. The error bars include only the random uncertainty. The bias uncertainty caused by calibration errors in Q and T_m does not influence the slope of the fitting line, is determined to be 34% and included in the total uncertainty shown in Fig. 5.

$$\kappa = \frac{\ln(R/r_0)}{2\pi t(R_m - R_c)}\alpha \qquad (17)$$

The obtained κ results are similar from measurements on the same CVD graphene suspended over four different 3.8 μm diameter holes. In Figure 5, we plot the as-obtained κ at each laser heating rate of the graphene monolayer suspended over one of the four holes versus T_m measured at that heating rate. The trend of decreased κ with increasing T_m reveals increased anharmonic scattering of those phonons that contribute to the measured κ. Because of the smaller contribution from the ballistic resistance component, the κ values obtained with the 50× objective are higher than the 100× objective for T_m < 450 K. Because l and thus the relative contribution from R_b decrease with increasing T_m, the κ values obtained with the two different objectives for T_m > 450 K become close to each other, and are thus expected to approach the intrinsic thermal conductivity of the suspended graphene. In addition, we note that phonons with $l > R$ are not heated by the laser beam because of the lack of scattering with photoexcited electron−hole pairs and other phonons, so that they do not contribute to thermal transport in the finite-size suspended graphene. Hence, the intrinsic thermal conductivity is expected to increase with the size of the suspended graphene based on the theoretical model of Klemens.[28] Nevertheless, the obtained thermal values are higher than the reported basal plane values of pyrolytic graphite[15,35,36] as shown in Figure 5.

This experiment has addressed two critical problems in thermal conductivity measurement of graphene using micro-Raman spectroscopy. First, the laser heating of the graphene suspended over a circular hole is measured directly by measuring the optical transmission through the graphene. The obtained optical absorption is close to the reported value measured in a similar geometry. Second, based on the thermal interface conductance of (28 + 16/−9.2) MW/m^2 K that is measured to be comparable to the recently reported values, the contact thermal resistance is determined to be considerably smaller than the measured thermal resistance of the suspended graphene. The obtained thermal conductivity of the supported graphene is (370 + 650/−320) W/m K, which is considerably smaller than that of suspended graphene in agreement with recent measurements of mechanically exfoliated graphene supported on SiO_2. The measured thermal resistances of suspended graphene at temperatures below 450 K reveal signatures of quasi-ballistic transport of low frequency phonons with mean free paths longer than the laser beam radius of 0.17 or 0.28 μm. The thermal conductivity of the suspended CVD graphene exceeds (2500 + 1100/−1050) W/m K near room temperature, and becomes about (1400 + 500/−480) W/m K at about 500 K. These values are higher than reported values for graphite.

Note: A Raman measurement of a large graphene flake suspended over a 44 μm diameter hole was reported during the final review stage of our paper. In that work,[38] the thermal conductivity was measured to be ∼630 W/m-K when the suspended mechanically exfoliated monolayer graphene was reported to be heated to ∼660 K at the laser spot and when the substrate was kept at ambient temperature. In addition, the laser spot radius from a 100x objective lens was estimated to be about 1 μm. If the laser spot radius was similar to our measured value of ∼178 nm for our 100x objective lens, then a higher thermal conductivity exceeding ∼850 W/m-K can be extracted from the data of ref 38. The measured thermal conductivity could also increase with a decreasing laser power and thus decreasing graphene temperature at the laser spot.

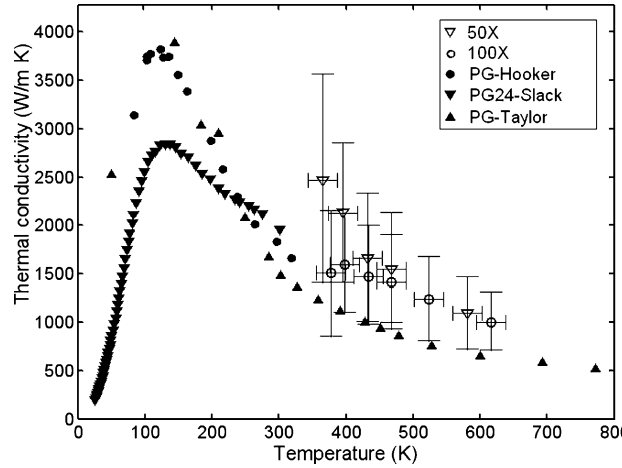

FIGURE 5. Thermal conductivity of the suspended CVD graphene measured using the 100× and 50× objective lens as a function of the measured graphene temperature. Also shown in comparison are the literature thermal conductivity data of pyrolytic graphite samples[15,35,36] as a function of temperature.

Acknowledgment. This work was supported in part by The University of Texas at Austin, the Texas Nanotechnology Research Superiority Initiative (TNRSI)/SWAN, Office of Naval Research awards N00014-08-1-1168 and N00014-10-1-0581, Department of Energy Office of Science award DE-FG02-07ER46377, and National Science Foundation award CBET-0553649.

REFERENCES AND NOTES

(1) Novoselov, K. S.; Geim, A. K.; Morozov, S. V.; Jiang, D.; Zhang, Y.; Dubonos, S. V.; Grigorieva, I. V.; Firsov, A. A. *Science* **2004**, *306*, 666–669.
(2) Geim, A. K.; Novoselov, K. S. *Nat. Mater.* **2007**, *6*, 183–191.
(3) Berger, C.; Song, Z. M.; Li, T. B.; Li, X. B.; Ogbazghi, A. Y.; Feng, R.; Dai, Z. T.; Marchenkov, A. N.; Conrad, E. H.; First, P. N.; de Heer, W. A. *J. Phys. Chem. B* **2004**, *108*, 19912–19916.
(4) Kim, K. S.; Zhao, Y.; Jang, H.; Lee, S. Y.; Kim, J. M.; Ahn, J. H.; Kim, P.; Choi, J. Y.; Hong, B. H. *Nature* **2009**, *457*, 706–710.
(5) Reina, A.; Jia, X. T.; Ho, J.; Nezich, D.; Son, H. B.; Bulovic, V.; Dresselhaus, M. S.; Kong, J. *Nano Lett.* **2009**, *9*, 30–35.
(6) Li, X. S.; Cai, W. W.; An, J. H.; Kim, S.; Nah, J.; Yang, D. X.; Piner, R.; Velamakanni, A.; Jung, I.; Tutuc, E.; Banerjee, S. K.; Colombo, L.; Ruoff, R. S. *Science* **2009**, *324*, 1312–1314.
(7) Novoselov, K. S.; Geim, A. K.; Morozov, S. V.; Jiang, D.; Katsnelson, M. I.; Grigorieva, I. V.; Dubonos, S. V.; Firsov, A. A. *Nature* **2005**, *438*, 197–200.

DOI: 10.1021/nl9041966 | *Nano Lett.* **2010,** *10,* 1645–1651

(8) Novoselov, K. S.; Jiang, D.; Schedin, F.; Booth, T. J.; Khotkevich, V. V.; Morozov, S. V.; Geim, A. K. *Proc. Natl. Acad. Sci. U.S.A.* **2005**, *102*, 10451–10453.
(9) Zhang, Y. B.; Tan, Y. W.; Stormer, H. L.; Kim, P. *Nature* **2005**, *438*, 201–204.
(10) Berber, S.; Kwon, Y. K.; Tomanek, D. *Phys. Rev. Lett.* **2000**, *84*, 4613–4616.
(11) Saito, K.; Nakamura, J.; Natori, A. *Phys. Rev. B* **2007**, *76*, 115409.
(12) Peres, N. M. R.; dos Santos, J.; Stauber, T. *Phys. Rev. B* **2007**, *76*, 205423.
(13) Mingo, N.; Broido, D. A. *Phys. Rev. Lett.* **2005**, *95*, 096105.
(14) Balandin, A. A.; Ghosh, S.; Bao, W. Z.; Calizo, I.; Teweldebrhan, D.; Miao, F.; Lau, C. N. *Nano Lett.* **2008**, *8*, 902–907.
(15) Slack, G. A. *Phys. Rev.* **1962**, *127*, 694–701.
(16) Ghosh, S.; Nika, D. L.; Pokatilov, E. P.; Balandin, A. A. *New J. Phys.* **2009**, *11*, 095012.
(17) Nair, R. R.; Blake, P.; Grigorenko, A. N.; Novoselov, K. S.; Booth, T. J.; Stauber, T.; Peres, N. M. R.; Geim, A. K. *Science* **2008**, *320*, 1308–1308.
(18) Seol, J. H.; Jo, I.; Moore, A. L.; Lindsay, L.; Aitken, Z. H.; Pettes, M. T.; Li, X. S.; Yao, Z.; Huang, R.; Broido, D.; Mingo, N.; Ruoff, R. S.; Shi, L. *Science* **2010**, *328*, 213−216.
(19) Cai, W. W.; Zhu, Y. W.; Li, X. S.; Piner, R. D.; Ruoff, R. S. *Appl. Phys. Lett.* **2009**, *95*, 123115.
(20) Calizo, I.; Balandin, A. A.; Bao, W.; Miao, F.; Lau, C. N. *Nano Lett.* **2007**, *7*, 2645–2649.
(21) If a flat top laser beam with radius r_0 is incident on the Au surface, the conduction thermal resistance of the gold support is $R_{Au} \approx 1/(4\kappa_{Au} r_0)$, where κ_{Au} is the thermal conductivity of the gold support. The temperature rise of the Au layer is $\Delta T = QR_{Au}$ where Q is the heat absorbed by the Au. For the 100× objective lens, the maximum incident power used to obtain Fig 2 with 3% absorptivity of the Au layer and κ_{Au} assumed to be reduced to 100 W/m K for the evaporated Au film from the bulk value of 317 W/m K,[37] the maximum temperature rise in the Au was found to be 4 K, which is much smaller than the 114 K value measured on the supported graphene at the same incident laser power.
(22) Greenberg, M. *Advanced Engineering Mathematics*, 2nd ed.; Prentice Hall: Upper Saddle River, NJ, 1998.
(23) Coleman, H.; Steele, W. *Experimentation and Uncertainty Analysis for Engineers*; Wiley: New York, 1989.
(24) Schmidt, A. J.; Chen, X. Y.; Chen, G. *Rev. Sci. Instrum.* **2008**, *79*, 114902.
(25) Chen, Z.; Jang, W.; Bao, W.; Lau, C. N.; Dames, C. *Appl. Phys. Lett.* **2009**, *95*, 161910.
(26) The maximum radiation transfer coefficient is obtained as $g_{rad} = \sigma T^5$ where σ is the Stefan-Boltzmann constant. The obtained g_{rad} reaches the maximum value of 15 Wm^{-2} K^{-1} at the upper limit of the measured graphene temperature of 650 K. Assuming that the energy accommodation coefficient of air molecules is 1 and ignoring the diffusive thermal resistance in the air, we calculate the maximum heat transfer coefficient to the surrounding air as the air interface thermal conductance per unit area, that is, $g_{air} = (nv/4)C$, where $n = P/k_B T_{air}$ is the number density of air molecules, $v = (3k_B T_{air}/m)^{1/2}$ is the root mean square velocity of air molecules, $C = 5k_B/2$ is the specific heat of diatomic molecules such as O_2 and N_2, k_B is the Boltzmann constant, P and T_{air} are the pressure and temperature of air molecules, and m is the mass of air molecules. The obtained g_{air} increases with decreasing T_{air} and approaches a maximum value of 1.08×10^5 Wm^{-2} K^{-1} for the lower limit of 300 K for this measurement and is orders of magnitude larger than g_{rad}. Thus, g_{rad} is negligible in comparison. The maximum g_{air} value is used to calculate the heat loss to the air $q_{air} = \int_0^R 2\pi r g_{air}(T(r) - T_a)dr$. Neglecting the contact resistance so that $T_1 = T_a$, we calculate q_{air} as a function of T_m using the measured r_0 values for the two objectives. For $T_m = 400$ K, the obtained q_{air} is 0.026 and 0.033 mW, or 5 and 6 times lower than the measured absorbed laser power Q at T_m 400 K for the 100× and 50× objectives, respectively. In addition, using $g = g_{air} = 1.08 \times 10^5$ W m^{-2} K^{-1} in eq. 8, we obtain thermal conductivity values that are within 6% of the values in Figure 5.
(27) Mills, A. F. *Heat Transfer,* 2nd ed.; Prentice Hall: Upper Saddle River, NJ, 1999; pp 100−103.
(28) Klemens, P. G. *Int. J. Thermophys.* **2001**, *22*, 265–275.
(29) Ma, Y. Z.; Stenger, J.; Zimmermann, J.; Bachilo, S. M.; Smalley, R. E.; Weisman, R. B.; Fleming, G. R. *J. Chem. Phys.* **2004**, *120*, 3368–3373.
(30) Siemens, M. E.; Li, Q.; Yang, R. G.; Nelson, K. A.; Anderson, E. H.; Murnane, M. M.; Kapteyn, H. C. *Nat. Mater.* **2010**, *9*, 26–30.
(31) Saha, S. K.; Shi, L. *J. Appl. Phys.* **2007**, *101*, 074304.
(32) Chen, G. *Phys. Rev. B* **1998**, *57*, 14958–14973.
(33) Chen, G. *J. Heat Trans.* **1997**, *119*, 220–229.
(34) Prasher, R. *Nano Lett.* **2005**, *5*, 2155–2159.
(35) Hooker, C. N.; Ubbelohde, A. R.; Young, D. A. *Proc. R. Soc. London, Ser. A* **1965**, *284* (1396), 17–19.
(36) Taylor, R. *Philos. Mag.* **1966**, *8*, 157–166.
(37) Incropera; D. *Fundamentals of Heat and Mass Transfered*, 5th ed.; J. Wiley & Sons: New York, 2002.
(38) Faugeras, C.; Faugeras, B.; Orlita, M.; Potemski, M.; Nair, R. R.; Geim, A. K. ACS Nano **2010**, DOI: 10.1021/nn9016229.

DOI: 10.1021/nl9041966 | *Nano Lett.* **2010,** *10,* 1645--1651